

## Research Article

# Dynamic Response of Bridge-Landslide Parallel System under Earthquake

Yu Liang,<sup>1,2</sup> Honggang Wu ,<sup>1,2</sup> Tianwen Lai,<sup>1</sup> Hao Lei,<sup>3</sup> Mingzhe Zhu,<sup>1</sup> Kun Ma,<sup>1</sup> Zhiyang Ji,<sup>1</sup> and Jiankai Ren<sup>1</sup>

<sup>1</sup>School of Civil Engineering, Lanzhou Jiaotong University, Gansu 730000, China

<sup>2</sup>Northwest Railway Academy Co., Ltd of CREC, Gansu 730000, China

<sup>3</sup>Department of Geotechnical Engineering, Tongji University, Shanghai 200092, China

Correspondence should be addressed to Honggang Wu; 271462550@qq.com

Received 22 October 2021; Revised 9 December 2021; Accepted 14 December 2021; Published 7 January 2022

Academic Editor: Cemal Ozer Yigit

Copyright © 2022 Yu Liang et al. This is an open access article distributed under the Creative Commons Attribution License, which permits unrestricted use, distribution, and reproduction in any medium, provided the original work is properly cited.

In order to further understand the instability mechanism and geohazard causation when the main sliding path of the slope body is parallel to the path of the bridge, the corresponding bridge-landslide parallel system is constructed for shaking table tests. This paper summarizes the combination forms of bridge-landslide model under different position and focused on the slope body located above the bridge deck. Firstly, based on the shaking table test results of El Centro (1940), the failure behavior of bridge-landslide parallel system was evaluated, and the changes of acceleration and deformation of bridge pile were subsequently analyzed. Then, the interaction bridge structure and sliding body were explained by the spectral features. The main conclusions are as follows. First, in the model test, the landslide belongs to the thrust-type landslide. Due to the barrier function of the bridge, the main failure site of landslide occurs in the middle and trailing edge of slope body. At the same time, the acceleration value of earthquake waves is 0.3 g, which is the key to this variation. Second, the acceleration response of the measuring points on the bridge pile and landslide increases with the increase of ground elevation. If the slope structure is damaged severely, the deformation response of weak interlayer is inconsistent with the surrounding soil structure. Third, with the increase of excitation power, the dominant frequency of bridge-landslide parallel system gradually transitions from low to high frequency rate, and the interaction of the parallel system weakens the influence of river direction on frequency. Finally, under the same working condition, the dynamic response of the measuring points has obvious regularity with the change of situation. But the response of the same points is not regular due to the different earthquake excitation intensity.

## 1. Introduction

China is a country with many geological calamities, and earthquake, landslide, debris flow, and other geohazards are very prominent in the western mountainous areas of China [1]. Furthermore, the construction of highway and railway often faces the problem of poor geological conditions, among which the landslide hazard is one of the typical types [2]. Additionally, since the western region is mostly hill and mountainous region, the bridge erection has become a common method to cross the adverse geological areas [3]. Therefore, how to accurately understand the dynamic response and failure characteristics of bridge-landslide under

earthquake action is an urgent problem that researchers need to solve.

In the last two decades, a large number of shaking table tests have been applied to the study of bridge-soil interaction. Yao et al. [4] studied the interaction behavior of pile-soil-superstructure model in saturated sand using a large shear box. Through the test, it is found that the ground behavior has a great impact on the soil superstructure. Tokimatsu et al. [5] studied the dynamic response of pile through shaking table test of structure pile sand model. It is found that when the period of structure is less than that of soil, the direct interaction force between pile and soil is in the same direction as the inertial force, and the stress received by

pile increases. Chau et al. [6] conducted an experimental study on the structural pile-soil model and observed the collision between the structural pile and the soil. Dou et al. [7] simulated the pile-soil dynamic response of single pile through shaking table test. The dynamic p-y curve measured by the experiment shows that the shallow depth has a high degree of nonlinearity and hysteresis under strong vibration and shows basic linear elastic behavior under low-level vibration. Gao et al. [8] studied the dynamic interaction between pile and soil under different amplitudes. The results show that the change of amplitude has a great influence on the dynamic response of pile foundation and foundation, such as the excess pore water pressure ratio in soil and the accelerated response of pile and soil. Wang et al. [9] conducted shaking table test of pile-soil structure using shear box. The test shows that the bending moment of pile pier is related to the scoured depth and increases with the increase of depth. Durante et al. [10] conducted shaking table tests to simulate a single pile or pile group model and found that the degree of coupling between the structure-soil system frequency and seismic waves determines the bending change of the pile. Shirgir et al. [11] studied the influence of pile-soil structure interaction (PSSI) on the earthquake response and dynamic characteristics of large-scale full model of super long-span cable-stayed bridge through earthquake wave, and the test results show that the interaction effect of pile-soil interface is gradually obvious with the increase of wave amplitude. The PSSI effect changes significantly with the change of wave frequency content. Zhang et al. [12] used the Yousuotun Bridge as a prototype to conduct multiple sets of large-scale shaking table model tests to study the force and deformation characteristics of bridge pier foundation piles under different waves, as well as the seismic performance and spectrum response laws of high and steep slopes. Luo et al. [13] used the method of risk analysis to explore the interaction between the Dongla Bridge and the Dongla Ancient Landslide. Chen et al. [14] studied the safety factor and failure mode of slope according to the interaction mechanism between seismic vibration and rainwater seepage through model test. In order to evaluate the landslide disaster induced by annual rainfall and earthquake, Nguyen et al. [15] proposed an integrated model with three modules: uncertainty analysis module, simulation module, and output module. Rajabi et al. [16] conducted a risk study of landslides in the area affected by the 1990 Manjil-Rudbar earthquake in Iran using back-propagation using artificial neural network. The abovementioned studies underline the importance of the effects of the PSSI.

Although there have been a lot of studies on the PSSI effect, most of the existing studies mainly consider the interaction between the foundation and bridge, and there are few studies on the interaction including the geohazard region and bridge. Therefore, the main focus of the present study is to explore the interaction of the bridge-landslide combination model.

At the same time, this paper collects and sorts out relevant literature and summarizes relevant engineering examples; it can be found that the relative positions of the bridge and the landslide determine the deformation

characteristics of the landslide and the stress mode of the bridge and ultimately determine the disease prevention and control engineering measures. For example, the landslide of Dongla Bridge [13] in Sichuan Province belongs to the bridge-landslide parallel system. The earthquake made the naturally quiet Dongla Bridge landslide accumulation structure looser, and it was revived under the action of rainfall and artificial excavation. Under the impact of the landslide, the bridge foundation collapsed, and the arch of the bridge deck cracked. The damage to the bridge near the mountainside was severe, and the damage to the bridge near the river was relatively small. The Chediguan Bridge [17] in Sichuan Province also belongs to bridge-landslide parallel system. Under the action of the earthquake, the upper part of the slope body collapsed, and the landslide occurred under the action of the collapsed body. Under the action of the landslide, the bridge deck was damaged, causing damage such as falling beams and overturning of bridge piers. The Zhengjiawan Bridge [18] in Shaanxi Province belongs to bridge-landslide orthogonal system, and the landslide type is the resurrection of old landslides. Under the action of the landslide, the bridge mainly caused damage such as transverse tension cracks and breakage of the block along the direction of the landslide. The damage of the bridge in the main sliding direction of the landslide is stronger than that on both sides and shows different damage patterns. The Chongqing Qianping Bridge also belongs to the bridge-landslide orthogonal system, and the landslide type is the resurrection of the old landslide. Under the action of the landslide, cracks occurred in the tie beams and piers of the bridge, and the failure strength of the bridge at different locations was different. The Lancang River Bridge in Yunnan belongs to the bridge-landslide oblique system, and the type of landslide is a steep and slippery slope. Under the influence of earthquake, rainfall, and artificial excavation, the bridge landslide was destroyed. The types of damage are those shown in parallel systems and those shown in orthogonal systems. The above case is shown in Figure 1.

The present study preliminarily categorizes the bridge-landslide system into the three following forms according to the angle between the main sliding direction of the landslide and the bridge axis: (1) bridge-landslide parallel system, (2) bridge-landslide orthogonal system, and (3) bridge-landslide oblique system. However, for lack of space, this study only demonstrates the bridge-landslide parallel system, as shown in Table 1. On this basis, the shaking table model test is carried out to analyze the dynamic response characteristics of landslide and bridge under seismic wave loading under different working conditions. The instability characteristics and mechanism of parallel landslide bridges are deeply studied. It provides experimental data support for the stability analysis theory and seismic design of bridge-landslide parallel system.

## 2. Materials and Methods

*2.1. Model Scaling Relations.* Because there are few direct engineering cases of bridge instability caused by earthquake-induced landslide revival, we did not specify a fixed

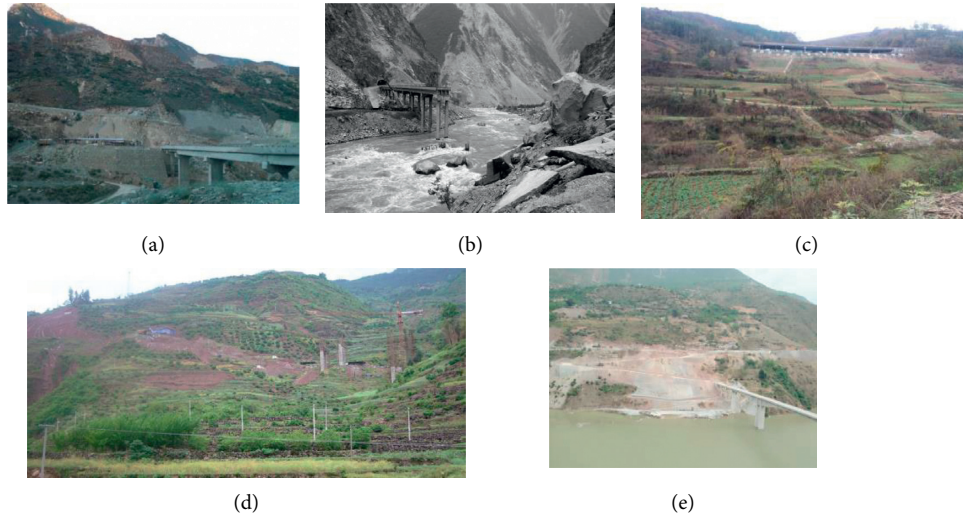


FIGURE 1: Typical case. (a) Dongla Bridge (Gang Luo et al. [13]). (b) Chediguan Bridge. (c) Zhengjiawan Bridge. (d) Qianping Bridge. (e) Lancang River Bridge.

TABLE 1: Bridge-landslide parallel system.

Diagram of the relative position of the bridge and the sliding surface		Deformation diagram	Bridge deformation characteristics	Classic case
Top view	Section view			
			The soil mass at the shear outlet slides and deforms seriously; collapse failure of pile foundation	Yousuotun Bridge along the Chenglan HSR [12]
			The slope deformation reduces the horizontal resistance of pile foundation, and the pile foundation has annular transverse cracks and pile foundation collapse	Zaoshugou Bridge (Lanzhou City) [19]
			The shear outlet is severely deformed, and there are obvious vertical and horizontal circular cracks in the pile foundation	Dongla Bridge (Sichuan Province) [13]

engineering prototype in this test, mainly to explore the regularity of failure law of bridge-landslide parallel system. But, considering the size of the shaking table model box and the application of the model in some practical construction projects, combined with the previous bridge engineering construction practice of relevant specifications, the gravity distortion model is selected [12]. This model test adopts Meymand's similarity law, with geometric size, density, and acceleration as the main control parameters, and its similarity constants are  $C_l=100$ ,  $C_\rho=1$ , and  $C_a=1$ , and the similarity ratio between the model and the prototype size is 1:100. According to the similarity theory and the basic principles of the abovementioned similar relationship design, the similarity constants of the remaining physical quantities are determined. The concrete parameters are shown in Table 2.

2.2. *Similar Materials.* Through the statistics of relevant cases, it is found that most bridge landslides are located in the southwest of China, and most of the southwest is red bed geology. Therefore, red bed geological materials were selected as model materials in this test. At present, the red bed model test mainly includes two methods: model test based on natural red bed and similar simulation test based on artificial materials [20]. The latter is chosen for this test. The design is based on relevant specifications (high-speed railway design code: TB10621-2014 [S].2015) and the previous experimental research; based on the orthogonal ratio design and indoor test, the final material ratio is as follows: (1) bed rock: red silt : quartz sand : cement : gypsum : water = 0.7 : 0.3 : 0.5 : 0.3 : 0.1; (2) sliding body: red silt : quartz sand : water = 0.7 : 0.2 : 0.1; and (3) sliding zone: quartz sand : soil : talc : water = 0.27 : 0.52 : 0.35 : 0.15. The concrete parameters are shown in Table 3.

TABLE 2: Scale factor.

Parameter type	Physical quantity	Dimension	Similarity ratio (prototype/model)
Physical dimension	Length ( $l$ )	$C_l$	1 : 100
	Mass density ( $\rho$ )	$C_\rho$	1 : 1
	Elastic modulus ( $E$ )	$C_E = C_l C_\rho$	1 : 100
	Poisson's ratio ( $\mu$ )	$C_\mu = 1$	1 : 1
Material characteristics	Gravity ( $\gamma$ )	$C_\gamma = C_\rho$	1 : 1
	Cohesion ( $c$ )	$C_c = C_l C_\rho$	1 : 100
	Internal friction angle ( $\varphi$ )	$C_\varphi = 1$	1 : 1
	Acceleration ( $a$ )	$C_a = 1$	1 : 1
	Time ( $s$ )	$C_t = C_l^{0.5}$	1 : 10
Load	Stress ( $\sigma$ )	$C_\sigma = C_l C_\rho$	1 : 100
	Strain ( $\epsilon$ )	$C_\epsilon = 1$	1 : 1
	Frequency ( $f$ )	$C_f = C_a^{0.5} C_l^{-0.5}$	1 : 0.1
Dynamic characteristics	Displacement ( $u$ )	$C_u = C_l$	1 : 100
	Speed ( $v$ )	$C_v = C_l^{0.5} C_a^{0.5}$	1 : 10
	Input acceleration ( $a$ )	$C_a = 1$	1 : 1
Structural characteristics	Frequency ( $f$ )	$C_f = 1$	1 : 1

These values represent the corresponding similarity ratio and its derivation process. At the same time, they are all formulas, so they are marked in italics.

TABLE 3: Physical and mechanical parameters of similar materials.

Similar material	Unit weight ( $\text{kN/m}^3$ )	Elasticity modulus ( $E$ ) (GPa)	Cohesion ( $c$ ) (kPa)	Internal friction angle ( $\varphi$ ) ( $^\circ$ )
Bed rock	17.5	0.04	6.9	32
Sliding body	17.2	—	4.6	22
Sliding zone	17.2	—	6.6	25

To obtain the transmission mechanism of the pier and pile affected by the surrounding landslide soil, the influence of the geometric size effect is considered. Referring to the research results of Yao [19] and others, a short pine pile is selected to simulate the bridge in this test.

We focus on the dynamic response of the bridge-landslide composite structure caused by earthquake-induced landslide revival, so the sliding surface is set in advance in the model design. The effectiveness of this method in simulating the initial sliding surface has been proved in previous studies (Large-Scale Model Test Study of Pipeline Crossing Landslide Interaction, by Jintao Liu [21]).

### 2.3. Test Setup

**2.3.1. Shaking Table Test Equipment.** The test was carried out using a hydraulic servo unidirectional seismic simulation shaker. This test uses a rigid model box with a clearance size of  $2\text{ m} \times 0.3\text{ m} \times 1.5\text{ m}$  (length  $\times$  width  $\times$  height), with tempered glass on both sides to observe the sliding process [22]. Lay a 5 cm thick special wooden slab at the back end of the landslide model to absorb seismic waves and reduce the impact of reflected waves [23]. The test setup is shown in Figure 2.

**2.3.2. Measurement System.** The acceleration sensor, strain sensor, and data acquisition system used in this experiment are products of Donghua Company. The acceleration sensor is a capacitive triaxial acceleration sensor, which is a capacitance sensor with a change in pole distance based on the capacitance principle. The strain sensor is a resistive strain



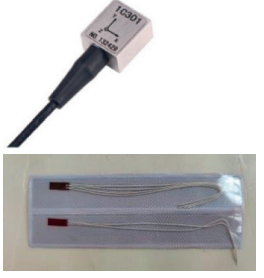
FIGURE 2: Shaking table test equipment.

gauge. Strain gauges are components used to measure strain composed of sensitive grids. Technical specifications are shown in Table 4.

**2.4. Layout Design of Measuring Points.** The preparation process of the combined model is “layered filling.” The model material is packed into the model box with a thickness of 10 cm layer by layer, and each layer is tamped according to the same method. Along with the model filling, the accelerometer and strain gauge are pasted on the bridge model structure in advance, and the bridge structure is installed at the target position, as shown in Figure 3. The layout of sensors in this experiment is shown in Figure 3. The landslide is 1.55 m long and 1 m high. The bridge model passes through three parts: sliding body, sliding belt, and surrounding rock. As shown in Figure 4, there are 12 acceleration sensors and 8 strain sensors. The acceleration sensor is mainly to capture the dynamic characteristics of



TABLE 4: Sensor.

Sensor type	Main parameter	Picture display
Acceleration sensor	Sensitivity: $0-42 \text{ mV/m}\cdot\text{s}^{-2}$ Measuring range: $0-20 \text{ m}\cdot\text{s}^{-2}$ Frequency response: $\text{Hz} + 3 \text{ dB}$ Resonant frequency: $>5.5 \text{ kHz}$	
Strain sensor	Resistance: $120.2 \pm 0.1 \Omega$ Sensitivity coefficient: $2.21 \pm 1\%$	

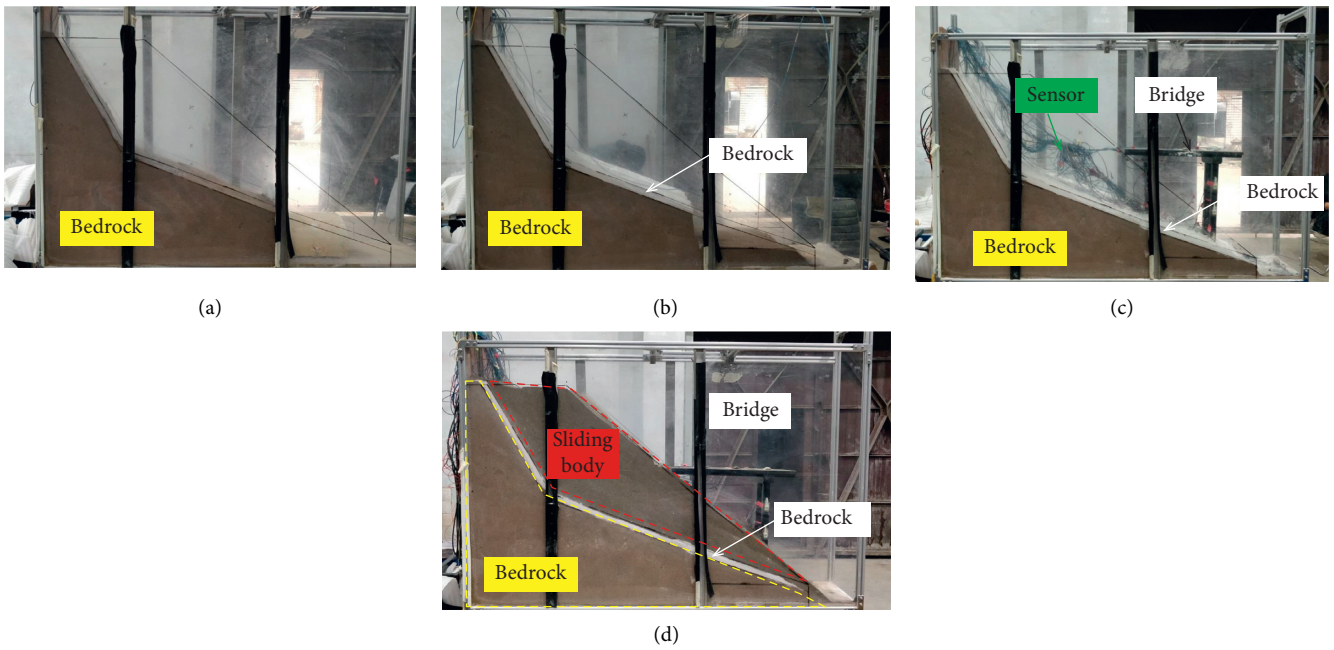


FIGURE 3: Filling process of model box. (a) Filling of bedrock. (b) Filling of slip zone. (c) Layout of model and sensor. (d) Model filling completed.

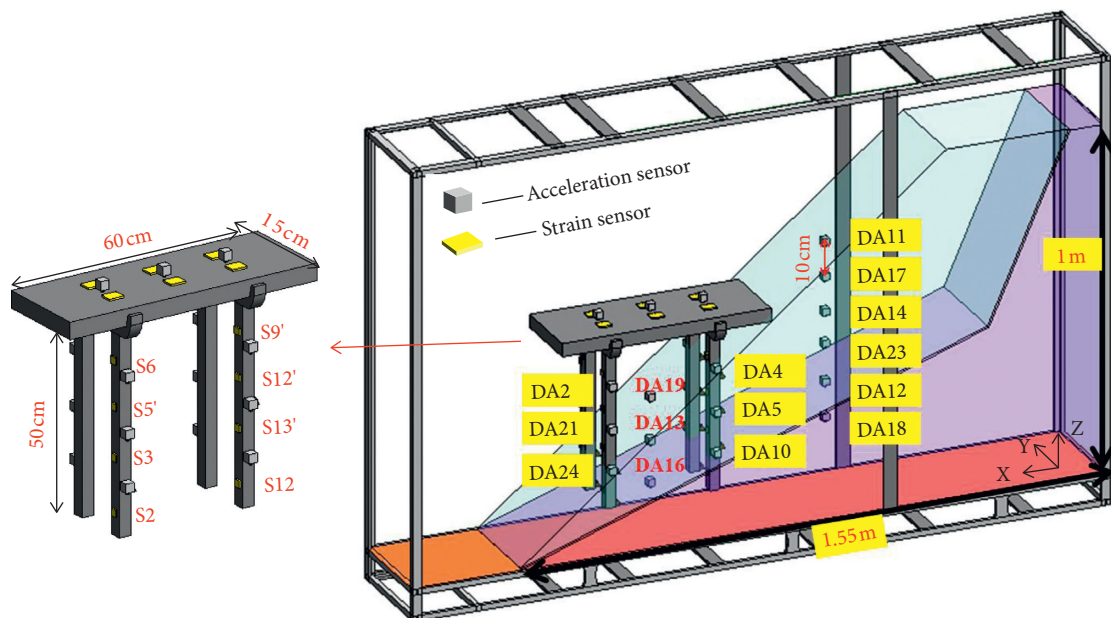


FIGURE 4: Sensor layout.

slope, pier column, and their joint parts. Therefore, three sections are arranged in Figure 4, and the position of the sensor in each section includes three different slope types: sliding body, sliding zone, and bedrock. The arrangement of strain gauge is mainly to avoid the deformation of bridge pier column under the action of landslide. At the same time, the layout spacings of the two sensors are the same. The acquisition instrument is mainly used to collect the electrical signal changes of bridge pile and surrounding soil.

**2.5. Loading Condition Design.** In the experiment, the seismic wave was simulated by continuously inputting sine wave, Kobe (1995), and El Centro (1940). This paper mainly analyzes the dynamic response of bridge-landslide system under horizontal unidirectional El Centro (1940) ( $x$  direction), as shown in Figure 5. The reasons for choosing these three waveforms are as follows: sine wave has strong regularity and is easy to observe; Kobe (1995) belongs to near-field earthquake, with special vibration mode, vertical and horizontal amplitude, strong intensity, and great damage, which is of great significance in the history of earthquake research; El Centro (1940) is the first seismic wave recorded in human history, which has specific and important historical significance.

This paper adopts the Poisson hypothesis commonly used in seismology to simulate multiple earthquakes [24]. It is assumed that the multiple earthquakes suffered by the structure are independent of each other and will not be affected. In addition, in order to consider the actual situation, the test ensures that the time interval between multiple earthquakes is long enough so that the structure has enough time to restore the acceleration and velocity to zero after the first earthquake [25].

### 3. Results and Analysis

**3.1. Initial Dynamic Characteristics of Test Model.** At the beginning of the test, white noise scanning is carried out to test the initial dynamic characteristics of the model, that is, natural frequency. The natural frequency of landslide is a parameter to describe the dynamic characteristics of landslide, which can be obtained by white noise excitation test [12]. The natural frequency can be expressed by the transfer function, and the frequency characteristics of the landslide acceleration response can be obtained by using the transfer function. The corresponding dominant frequency on the spectrum is the natural frequency of the landslide. Figure 6 is the spectrum of white noise at measuring point DA14, and the corresponding natural frequency is 16.63 Hz.

**3.2. Deformation and Failure Characteristics of the Model.** This article is carried out under the condition that the slope body has been loaded with the KOBE wave. The state of the test model after loading the KOBE wave is shown in Figure 7(a). According to the observation of the changes of the slope under KOBE loading, it is analyzed that the failure of the landslide is due to the upper rock layer slides and squeezes the lower part to produce deformation, which

eventually leads to the sliding. In addition, the surface of the sliding body is undulating, and there are deposits in the slope section, which conform to the characteristics of thrust load caused landslide. Therefore, it can be determined that the failure form of the landslide is thrust load caused landslide. Under this premise, the EL Centro wave is loaded. Under the loading of low-intensity earthquake waves (0.1–0.2 g), the main causes are the deformation and development of the original cracks and the increase of cracks in the middle of the lower sliding zone of the landslide. The detailed information is shown in Figure 7(a).

Under the loading of earthquake wave (0.3 g), the slope deformation gradually develops from the local deformation of the trailing edge to the overall sliding of the slope. With the continuous development of the width and depth of the cracks in the trailing edge of the slope, the deformation range gradually expands and advances from the back to the front, and the rear part of the slope gradually slides forward. As a result, the shear dislocation zone begins to appear on both sides of the boundary of the rear part of the landslide, and the lateral shear tension cracks occur. As the deformation continues to increase, the sliding range of the slope gradually increases from the rear edge to the front, and the shear cracks in the flank are arranged in the echelon and extend forward until they reach the front of the slope. The trailing edge of the slope produces large deformations, and the cracks are abundant. The cracks are mainly distributed in the sliding body at the middle and trailing edge of the landslide and tend to connect into a line. The strike is roughly similar to the sliding belt and is distributed in the upper part of the sliding belt. There is no obvious change in the sliding body part where the bridge model is located.

The reason for the analysis is that the bridge column has a certain protective effect and plays a role similar to that of the “antisliding pile.” The specific phenomenon is shown in Figure 7(b).

Under the action of high-strength (0.4 g, 0.6 g) earthquakes, the cracks of the landslide continued to develop, and the cracks in the sliding body were gradually connected into a line to form a secondary sliding surface and gradually extended to the sliding body at the bridge model. The cracks in the sliding zone are also increasing, mainly distributed in the rear edge and the middle. The main reasons for this distribution are the deformation characteristics of the thrust load caused landslide and the blocking effect of the lower bridge, as shown in Figures 7(c) and 7(d).

From the overall situation of landslide change, the whole is consistent with the deformation characteristics of thrust load caused landslide. 0.3 g seismic wave is the turning point of landslide change, which ends the stage of crack development under low-intensity seismic wave loading and opens the stage of large deformation of landslide.

#### 3.3. Acceleration Response Analysis of Landslide Slope

**3.3.1. Acceleration Time-History Dynamic Response Characteristics.** Because the acceleration time-history curves under all working conditions are roughly the same,

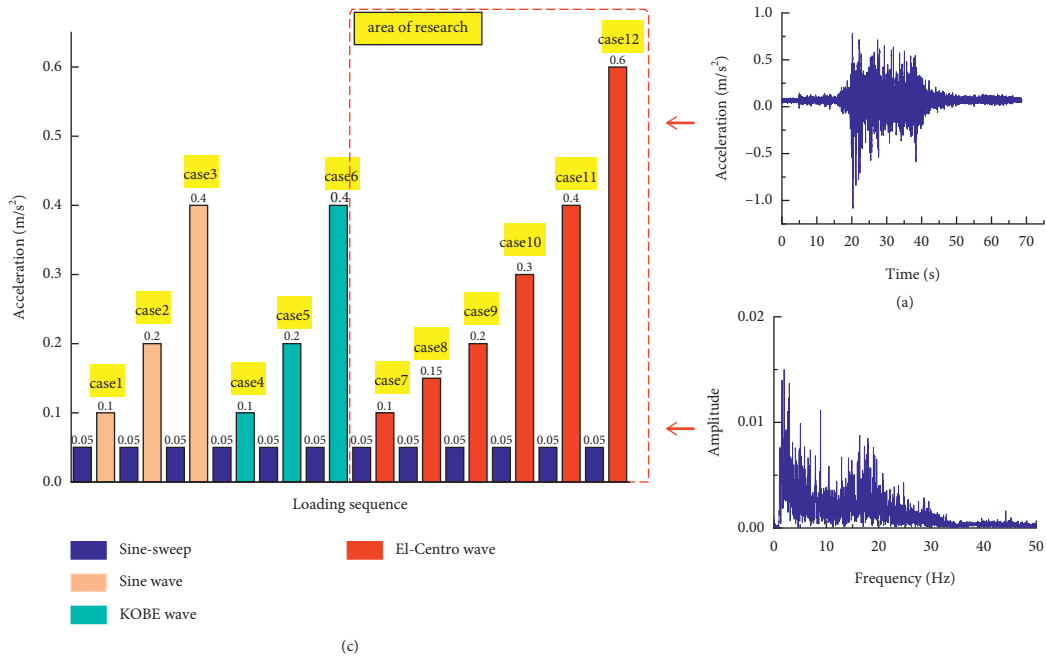


FIGURE 5: Loading condition design. (a) Time history of El Centro. (b) Fourier spectrum of El Centro. (c) Loading sequence of the shaking table test.

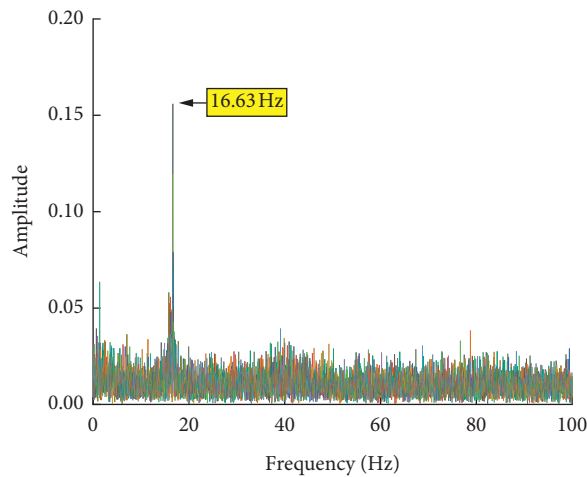


FIGURE 6: White noise spectrum (DA14).

the acceleration time-history curve at 0.4 g is selected for a detailed description. At the same time, it is stipulated that the section where the measuring point DA11 is located is section 1, and the section where the measuring point DA19 is located is section 2.

Firstly, comparing the acceleration time-history curves of different elevation measuring points in Figure 8(a), it can be seen that the maximum peak response time of each measuring point in section 1 shows hysteresis rule, and, with the increase of elevation, the peak response time of the measuring point also lags relatively. The data of DA11 has an obvious error, so it is not analyzed. The waveforms of the acceleration time history curves of the remaining measurement points are consistent with the waveform law of the

EL Centro wave. At the same time, the acceleration response of the upper slope of the sliding zone increases with the increase of the elevation of the measuring points, and the acceleration response at the sliding zone is stronger than that of the measuring points in a certain range on both sides of the sliding zone.

Secondly, comparing the acceleration time-history curves of different elevation measuring points in Figure 8(b), we can see that the maximum peak response time of each measuring point in section 2 also presents hysteresis. At the same time, compared with the maximum response time of each measuring point in section 1, it is found that the horizontal propagation of seismic waves on the landslide slope also presents hysteresis. The acceleration response of

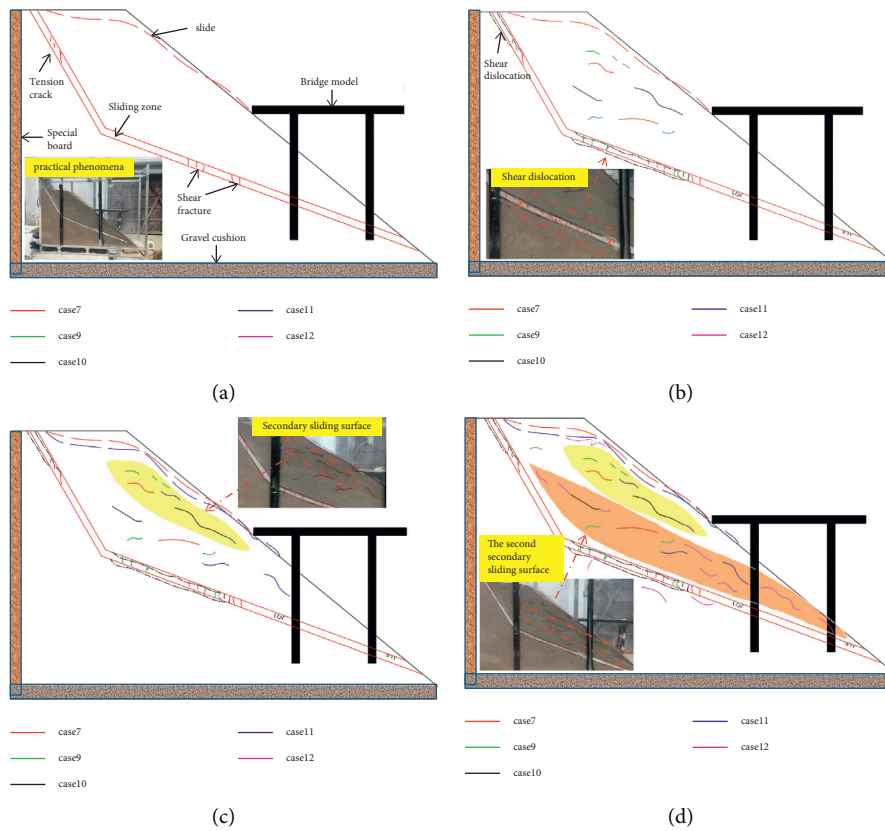


FIGURE 7: Experimental phenomena of landslides at different stages. (a) Phenomenon of initial slope test. (b) Test phenomenon of case 10 (0.3 g). (c) Test phenomenon of case 11 (0.4 g). (d) Test phenomenon of case 12 (0.6 g).

each measuring point shows the law of weakening with the increase of elevation, which is different from that of section 1. The reason is that the middle part of the bridge is mainly affected by the bottom-up propagation of seismic waves due to the barrier effect of piers.

In general, from the acceleration time history curve, there is a lag in the occurrence time of acceleration maximum peak in both vertical and horizontal directions. At the same time, the existence of bridges will change the propagation law of seismic waves in slopes.

### 3.3.2. Correlation Analysis of Acceleration Response.

Correlation refers to the degree of correlation between two variables. Generally, two variables have one of the three following relationships: positive correlation, negative correlation, and irrelevance. It can measure the closeness of two variable factors. In this paper, the dynamic response of the pile foundation in the bridge-landslide system in the red mudstone area under the action of earthquake is studied by the correlation analysis of the three factors of seismic excitation intensity, acceleration response, and corresponding spatial location. The commonly used correlation coefficient judgment table is shown in Figure 9(a).

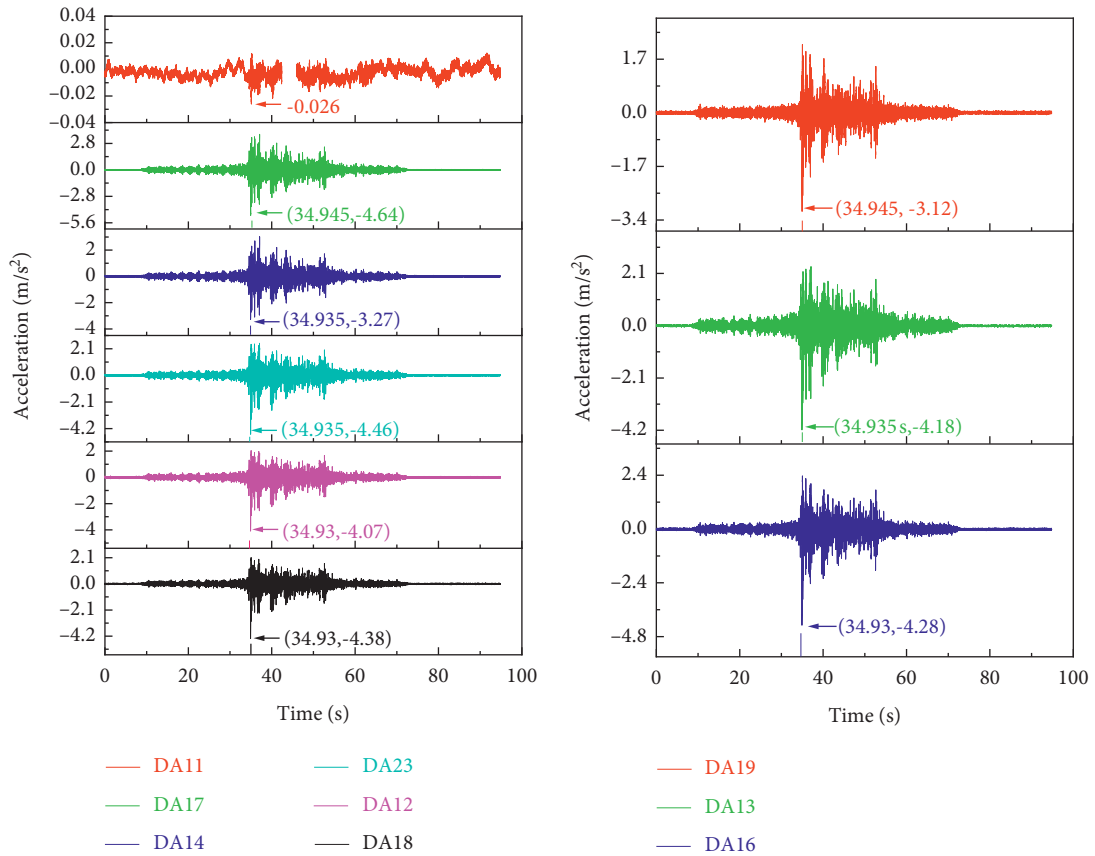
Because the sampling frequency of acceleration in this test is 200 Hz, the main shock loading time of seismic wave is 1.10 min, and the amount of data is large; if all the correlation analysis is carried out, it will cause unnecessary

storage and calculation. But if the sampling interval is too large, it will cause “spectrum aliasing effect.” Therefore, choosing a better sampling interval is the first problem to be solved. According to the research of Aimin et al. [26] and others, combined with the actual situation, the data after the maximum peak response time of acceleration time history curve under various working conditions are selected in the sampling space, as shown in the marked area in Figure 9(b). The sampling interval was 0.1 s, and 176 pieces of data were selected for analysis.

Figure 9(c) shows the correlation analysis of acceleration amplitudes at different elevation points on section 1 in the middle of the slope under five different earthquake excitations of 0.1 g, 0.15 g, 0.2 g, 0.3 g, and 0.4 g. The yellow area is the fitting curve of the correlation coefficient between the bottom measuring point and the remaining measuring points. The pink area is the fitting curve of the correlation coefficient of DA12 to DA23, DA14, and DA17; the green area is the fitting curve of the correlation coefficient of DA23 to DA14 and DA17; the gray area represents the correlation coefficient of DA14 to DA17.

It can be found from Figure 9 that as the distance between the measuring points increases (decreases), the correlation between the measuring points decreases (increases). Among them, the correlation coefficients between the measuring points under the excitation of 0.15 g, 0.2 g, and 0.4 g are all greater than 0.8, indicating that there is a high degree of positive correlation between the acceleration

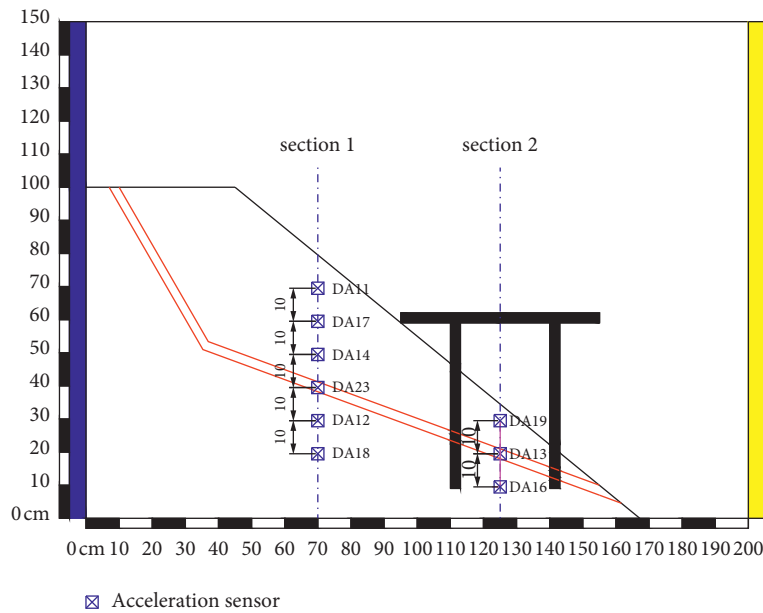




a

(a)

(b)



(c)

FIGURE 8: Acceleration time-history curves of different elevation measuring points in different sections (0.4 g). (a) Acceleration time-history curves of different elevation measuring points in section 1. (b) Acceleration time-history curves of different elevation measuring points in section 2. (c) Sensor location map.

Range of correlation coefficient	$r=0$	$ r  < 0.3$	$ r  = 0.3\sim 0.5$	$ r  = 0.3\sim 0.5$	$ r  = 0.3\sim 0.5$	$ r  = 1$
Degree of correlation	Uncorrelated	Weak correlation	low correlation	significant correlation	Highly correlated	Completely relevant

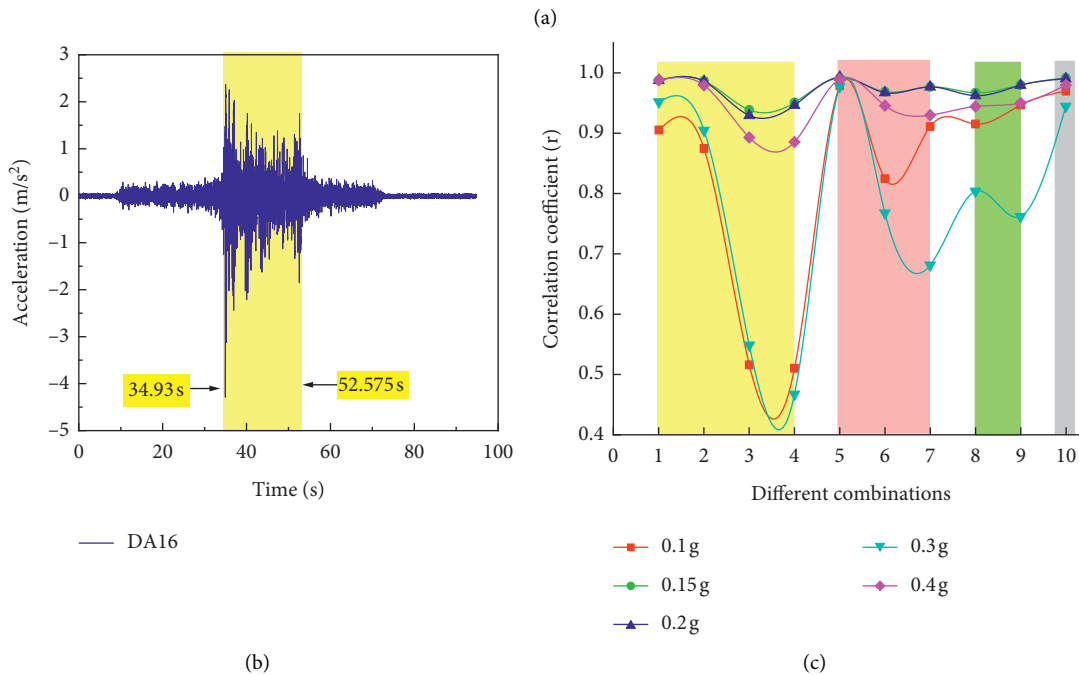


FIGURE 9: Correlation analysis. (a) Correlation coefficient. (b) Schematic diagram of data sampling space. (c) Correlation coefficient diagram of bridge pile measuring points under different working conditions (Note: 1–10, respectively, indicate different correlation analysis combinations, namely, DA18-DA12, DA18-DA23, DA18-DA14, DA18-DA17, DA12-DA23, DA12-DA14, DA12-DA17, DA23-DA14, DA23-DA17, and DA14-DA17).

responses of the measuring points. Under the excitation of 0.1 g and 0.3 g earthquakes, the correlation between the measuring points varies greatly. The correlation between the measuring points on the lower part of the sliding zone and the upper part of the sliding zone is between 0.4 and 0.8, and the correlation between the measuring points under the excitation of 0.3 g earthquake is the worst. This is because the slope just experienced the seismic excitation of the KOBE wave at the time of case 7 (0.1 g). Although only 0.1 g EL Centro wave was loaded, due to the difference of the two excitation types, a certain response occurred inside the slope. The particularity of case 10 (0.3 g) is due to the fact that the excellent frequency of the slope is very close to the natural frequency of the slope and the severe deformation of the sliding belt in this working condition.

This reflects the influence of the spatial position on the dynamic response of the measuring points. However, by analyzing the correlation between the earthquake excitation intensity and the dynamic response of the measuring points, it is found that there is no obvious correlation between the dynamic responses of the same measuring points under different earthquake excitation intensities.

### 3.4. Acceleration Response Analysis of Bridge Pile Foundation

3.4.1. Acceleration Response Analysis of Bridge Pile Foundation on Mountainside. Because the measuring points of the bridge pile located on the slope slide can provide different peak accelerations, through analyzing the above effect on the different working conditions (Figure 10), conclusions are as follows:

- (1) Except for case 10 (0.1 g) and case 12 (0.4 g), the peak size relationship is top > middle > bottom, which indicates that the acceleration response on the pier increases with the increase of the elevation of the measuring points.
- (2) The relationship of peak acceleration at working case 10 and case 12 is top > bottom > middle, and the value is much larger than other working conditions. Among them, the response of slope body and bridge under working case 10 (0.3 g) is the strongest or even greater than the response of EL Centro wave (0.6 g). This is because the predominant frequency of the pier is 16.38 Hz under case 10 (0.3 g), which is

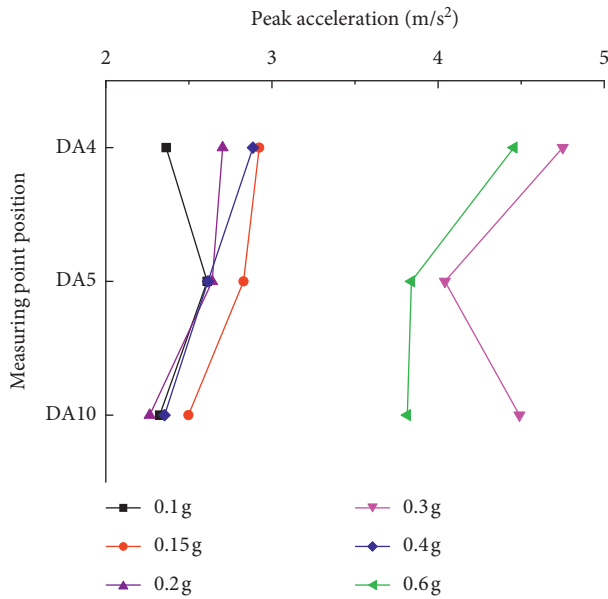


FIGURE 10: Peak acceleration at different measuring points of bridge pile on mountainside.

basically consistent with the natural frequency of the slope (the frequency spectrum of the measuring point DA4 is shown in Figure 11, and the predominant frequency of other measuring points on the pier is also basically consistent). It is attributed to the serious destruction of sliding zone.

This indicates that the weak interlayer and the surrounding soil will present an incompatible deformation response.

3.4.2. *Acceleration Response Analysis of Bridge Pile Foundation on Riverside.* The peak acceleration at different measuring points of the bridge pile on the riverside is shown in Figure 12. Through the analysis of the maximum peak acceleration of each measuring point on the riverside of the left bridge pier in front of the bridge under different working conditions, it can be concluded that the acceleration is top > middle > bottom. This shows that, with the increase of elevation, the acceleration response of the pier increases; and the response of case 10 (0.3 g) is the strongest. This is due to the fact that the predominant frequency of the pier is consistent with the natural frequency of the slope at case 10 (0.3 g).

In a word, we have the following:

- (1) Generally, the acceleration response of the measuring points on the bridge pile increases with the increase of elevation. However, when the sliding zone is seriously damaged, the acceleration response law of the measuring points on the pile will change. Research shows that the weak interlayer and the surrounding soil will present an incompatible deformation response.

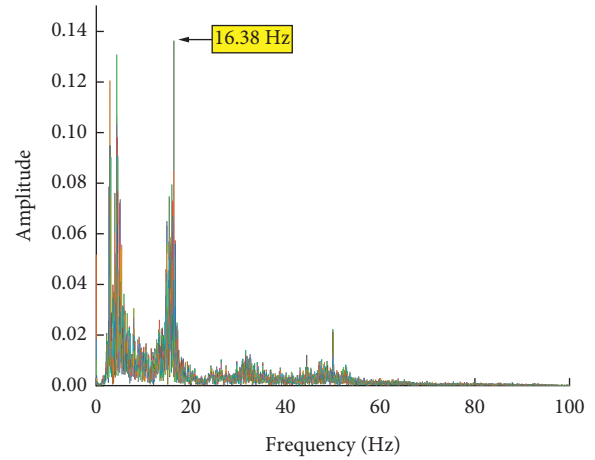


FIGURE 11: Spectrum of DA4 measuring points.

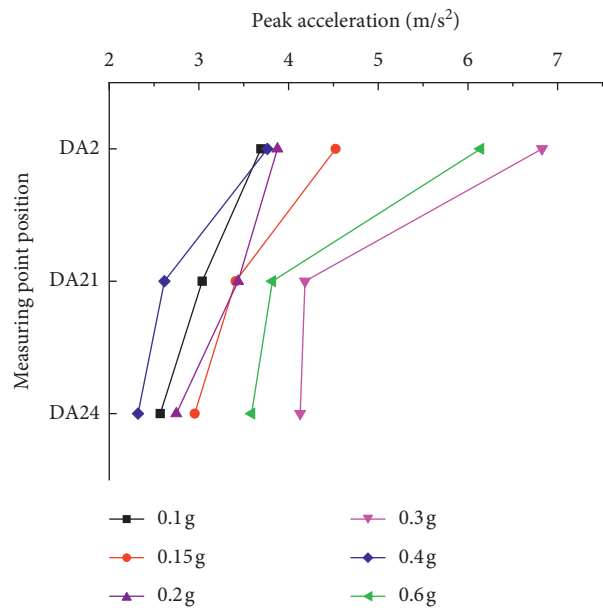


FIGURE 12: Peak acceleration of bridge pile on riverside at different measuring points.

- (2) The acceleration response of the measuring points located on the slope side is greater than the acceleration response of the measuring points on the riverside. It is indicated that the mountainside pile has a certain protective effect on the riverside pile.

3.4.3. *Correlation Analysis of Acceleration Response.* As shown in Section 3.3.2, the correlation analysis of the acceleration of the measuring points on the bridge pile is carried out. Figure 12 shows the correlation coefficient between the measuring points under different working conditions. The left side of the red line is the riverside pile measuring points, and the right side is the mountainside pile measuring points. The following can be seen from Figure 13:

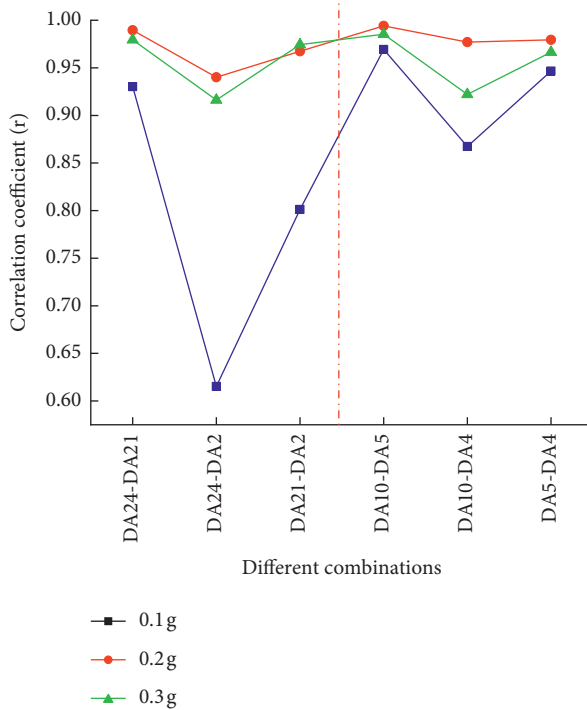


FIGURE 13: Correlation coefficient diagram of bridge pile measuring points under different working conditions.

- (1) No matter on the riverside or on the mountainside, the correlation between the observation points decreases (increases) with the increase (decrease) of the distance between the observation points. The reason for the analysis is that this is related to the propagation law of seismic wave from bottom to top and energy dissipation. Moreover, the correlation of the measuring points of the pier column on the mountainside is stronger than that on the riverside. It is caused by the protective effect of the pier column on the hillside.
- (2) The stronger the earthquake excitation is, the stronger the correlation between the measuring points is. It can be seen from the figure that only under working condition 7 is the correlation coefficient between DA24 and DA2 0.6153. With the increase of working condition, the correlation coefficient of each measuring point is greater than 0.8, showing a high correlation. The reason for the analysis is that when the seismic excitation is low, due to the energy absorption effect of the pier and the protective effect of the slope on the pile, with the increase of elevation, the correlation between the upper and lower measuring points of the pier is poor. However, the protective effect of pier and slope is limited, so, with the increase of seismic excitation intensity, the influence of pier and slope decreases, and the correlation of measuring points on pier increases.

This reflects the influence of the spatial position on the dynamic response of the measuring point. However, by analyzing the correlation between the seismic excitation intensity and the dynamic response of the measuring points,

it is found that there is no obvious correlation between the dynamic responses of the same measuring points under different seismic excitation intensities. This phenomenon shows that different excitation earthquake waves have different effects on bridge reconstruction.

Table 5 shows the correlation coefficient of the pier column measuring points on the mountainside and riverside. The following can be found from Table 5:

- (1) The stronger the earthquake excitation is, the stronger the maximum peak correlation between the measuring points is.
- (2) It can be seen from the bold correlation coefficient in Table 5 that, with the enhancement of earthquake excitation, the elevation corresponding to the correlation coefficient of each measuring point on the mountainside bridge pile and the riverside gradually increases. This is due to the protective effect of slope and mountainside pier on riverside pier. When the earthquake excitation is low, the protective effect is greater, but, with the increase of earthquake excitation, the protective effect gradually weakens.

**3.5. Strain Response Analysis of Bridge Pier.** Through the analysis of the peak strain of each measuring point of the bridge pile on the side of the mountain (Figure 14(a)) under different working conditions, it can be found that the magnitude of the strain peak under each working condition is  $S12 > S13 > S12'$ . Due to the failure of the upper measuring points of  $S12'$ , it can only be shown that the deformation of the bridge pile in the soil near the mountain decreases with the increase of elevation. The reason for the analysis is that the three measuring points are all in the sliding body, and the seismic wave is transmitted from the bottom to the top.  $S12$  is the first place to contact the seismic wave, and, with the propagation of the earthquake wave, the energy slowly decays and the slope absorbs energy, so the deformation here is the largest.

Through the analysis of the peak strain of each measuring point of the bridge pile on the riverside (Figure 14(b)) under different working conditions, it can be found that, under different working conditions except case 10 (0.3g), the magnitude of the maximum strain peak is basically  $S6 > S3 > S2 > S5'$ . The particularity of  $S5'$  is due to the location of the measuring points and the failure form of the landslide. It reflects the soil-pile interaction.

In case 10 (0.3g), the predominant frequency of the bridge model is similar to the natural frequency of the slope, so it is different from the other working conditions [27].

In case 12 (0.6g), the response at  $S2$  is superior to that at  $S3$ . This is caused by two factors. First, after the loading of the previous conditions, the soil at the front end of the slope accumulates, which makes the pier relatively stable, and the influence of the slope's pushing force is reduced. Second, the seismic wave is transmitted from the upper part of the lower direction, while  $S2$  is the first place to contact the seismic wave. This is why  $S2$  is stronger in testing.

From the analysis of 3.4 and 3.5, it can be clearly seen that the acceleration response and strain response of the

TABLE 5: Correlation coefficient of measuring points of pier column at mountainside and riverside under different working conditions.

Case 7 (0.1 g)			
	DA2	DA21	DA24
DA4	0.8815	<b>0.96271</b>	0.86511
DA5	0.82448	<b>0.92728</b>	0.92411
DA10	0.71416	0.86735	<b>0.9443</b>
Case 9 (0.2 g)			
	DA2	DA21	DA24
DA4	0.96572	<b>0.99161</b>	0.98325
DA5	0.95939	0.9821	<b>0.98709</b>
DA10	0.95505	0.97811	<b>0.98955</b>
Case 11 (0.4 g)			
	DA2	DA21	DA24
DA4	<b>0.98185</b>	0.97765	0.92489
DA5	0.96234	<b>0.99349</b>	0.98429
DA10	0.9187	0.97554	<b>0.99683</b>

Because these values are the largest in each row, they reflect some characteristics of the correlation law between the two sensors. And this feature is also described in detail in this text. Therefore, these values are bold.

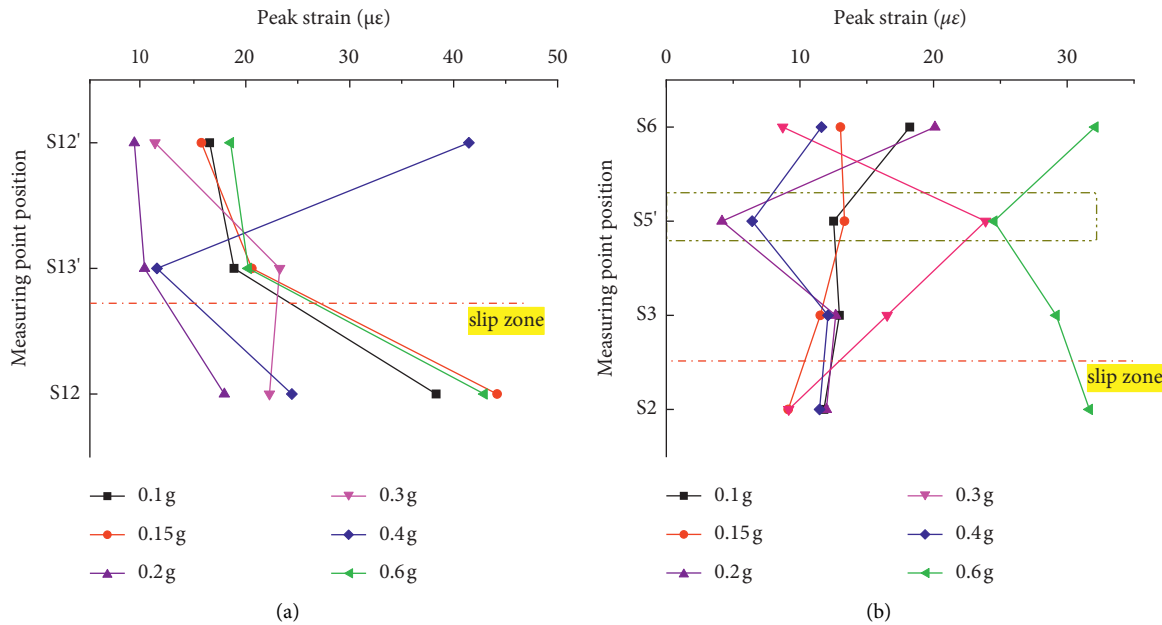


FIGURE 14: Peak strain at measuring points of bridge pile under different working conditions. (a) Pier column on the side of the mountain. (b) Pier column on the riverside.

measuring points on the pier are different. The acceleration response of the pier column on the hillside increases with the elevation of the measuring point, while the strain response presents the opposite law. The acceleration response on the riverside bridge pile increases with the increase of the elevation of the measuring point, and the strain response also presents the same law. It can be found that the difference between the acceleration and strain law of the measuring points is mainly reflected in the mountainside bridge pile.

#### 4. Discussion

4.1. *Spectrum Characteristic Analysis.* The bridge-landslide interaction site is mainly near the mountainside of the bridge. From the previous article, it can be known that the difference

between the acceleration and strain law of the measuring points on the bridge pile is mainly reflected in the pile located on the slope slide [28]. Therefore, the acceleration spectrum characteristics of the measuring points in section 1 (DA17, DA18), the measuring points on the hillside pier column (DA4, DA10), and the measuring points in section 2 (DA19, DA16) are selected for comparative analysis to discuss the bridge-landslide interaction. Due to the limited space, only the spectrum diagrams of the measure points at the middle of the slope (DA17) are listed below, as shown in Figures 15(a) and 15(b). Figures 15(b) and 15(c) show the excellent frequency of other measuring points.

In the spectrum, 50 Hz is the interference frequency of AC in China, which is not caused by seismic waves. When the excitation intensity is 0.15 g, the dominant frequency of



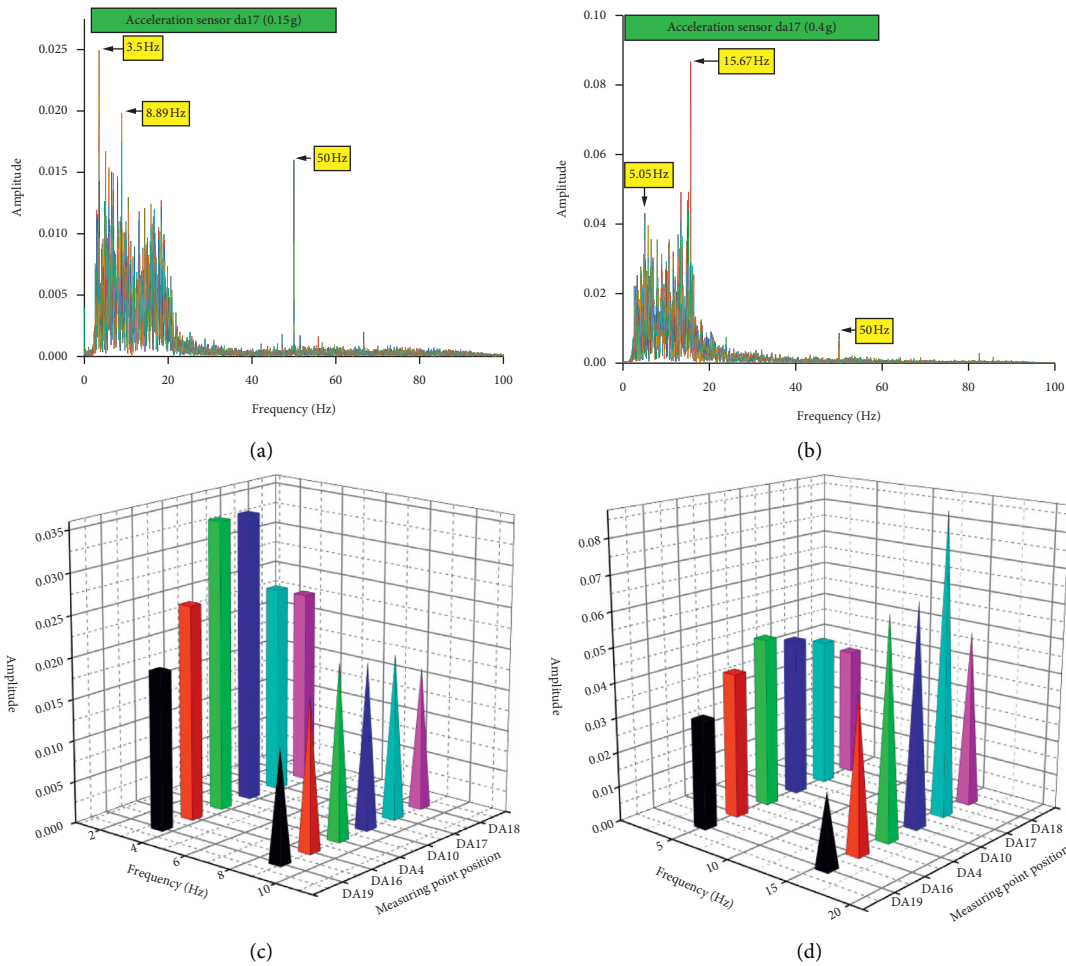


FIGURE 15: Excellent frequency of selected measuring points under different cases. (a) Spectrum curve of DA17 (0.15 g). (b) Spectrum curve of DA17 (0.4 g). (c) Excellent frequency of selected measuring points (0.15 g). (d) Excellent frequency of selected measuring points (0.4 g).

slope response acceleration is 3.5 Hz and there is also a strong amplitude near 8.89 Hz, which is close to the dominant frequency of input wave, indicating that the transformation effect of slope on input wave is very weak. At the same time, the amplitude at the top of the slope is larger than that at the bottom, reflecting the elevation amplification effect. When the excitation intensity is 0.4 g, it can be observed that the excellent frequency migrates to 15.67 Hz, and a strong amplitude also appears at 5.05 Hz. At this time, it is quite different from the spectral characteristics of the input wave. Combined with the above analysis of the dynamic characteristics of the slope, it is indicated that the internal structure of the slope has changed at this time. At the same time, the amplitude of the slope top is greater than that of the bottom, which also reflects the elevation amplification effect.

Combined with the natural vibration frequency of the slope in 3.1, it can be found that, with the increase of excitation intensity, the superior frequency gradually approaches the natural vibration frequency of the slope, which also explains why the slope body changes gradually increase with the increasing seismic excitation.

At the same time, the change trend of the remarkable frequency of the measuring points on the hillside pier

column is basically the same as that of the measuring points in the slope.

It is shown that the change trends of the bridge pile located on the mountainside and slope under earthquake are basically the same, which is related to two factors: the buried depth of mountainside pier column and the first time contact with earthquake wave and slope thrust.

However, the measuring points in section 2 (DA19, DA16) are consistent with the other two only when the seismic excitation intensity is low. When the seismic excitation intensity increases, the spectrogram of the measuring points of section 2 (DA19, DA16) shows a different law: the excellent frequency does not show a tendency to change to high frequency. This is due to the bridge-landslide interaction. When the bridge structure is located in an earthquake-affected site, the inertial force generated by the bridge collapse structure will be transmitted to the ground soil through the pile foundation, which is the cause of soil deformation. Then, the deformation of the soil mass will affect the pile foundation, and the deformation of the foundation will cause deformation and vibration of the bridge structure. In this procedure, only part of the energy is absorbed by the structure, while the other part of the energy is transmitted to the landslide body through wave radiation, which is

consumed by the soil and the bridge structure. This increases the damping of the interaction system and prolongs its natural vibration period, so that the excellent frequency at the riverside is still in the low frequency region. These will adversely affect the bridge-landslide interaction system.

**4.2. Failure Model.** In this test, under the action of earthquake wave, a large number of subsidence cracks are produced at the top of the slope body and the slip zone. At the same time, the slope structure is subject to tensile crack, as well as oblique shear slip change, and weak zones are formed. Weak zones generally exist at the geotechnical boundary. The bridge-pile structure also produces certain creep deformation. In case of small deformation, the deformation of sliding mass is not obvious. As a sensitive structure, the small deformation of landslide may have a great effect on the bridge pile, thus forming a dynamic response mode of micro progressive slope and macro deformation of column.

Through the above analysis and combined with the case of Table 1, the disaster mode of bridge-landslide parallel system can be summarized. The paper shows the progressive destruction of slope and the cooperative deformation mechanism of the bridge structure. First of all, there are two main types of landslides: one is the ancient landslide accumulation, and the other is the high, steep, and slippery slope [29]. There are three main reasons affecting the deformation of bridge-landslide system: bridge construction, rainfall, and earthquake. This paper mainly discusses the influence of earthquake. The earthquake makes the landslide resurrect or slide, forming multiple weak zones in the sliding body and then developing into shallow sliding surface and deep sliding surface. Among them, the deep sliding surface is basically at the geotechnical boundary. The interaction between bridge and landslide makes the bridge and landslide prone to resonance, or the impact of landslide directly damages the bridge. Finally, the failure forms of the bridge are dumping, falling beam, and so on, but the destruction process of the bridge and the destruction process of the landslide are gradual and coordinated, not sudden or separated from each other.

## 5. Conclusion

Through a series of shaking table model tests, the dynamic response and instability characteristics of the bridge-landslide parallel system under EL Centro wave are studied. Through a series of shaking table model tests, the acceleration and strain responses of bridges and landslides are analyzed. At the same time, the bridge-landslide interaction is analyzed through correlation analysis and spectrum analysis. The conclusions can be got as follows:

- (1) Based on the record and analysis of the slope failure behavior, the failure mode of landslide is confirmed. The failure mode of landslide belongs to the thrust-type landslide, and there are three main stages: the destruction of the trailing edge, the shear failure of the sliding surface, and the formation of the

secondary sliding surface. The progressive failure of the slope body and the synergistic deformation mechanism of the bridge structure are shown.

- (2) In general, whether it is a slope or a bridge pile, the acceleration response increases as the elevation increases. However, when the structure of the sliding zone is severely damaged, the acceleration response rule will change accordingly. The weak interlayer and the surrounding soil will generate uncoordinated deformation response. It is indicated that there is an inconsistent deformation response between the weak interlayer and the surrounding soil.
- (3) The acceleration response of the bridge pile on the hillside increases with the elevation of the measuring points, while the strain response presents the opposite law. The acceleration response on the riverside pile increases with the increase of the elevation of the measuring point, and the strain response also presents the same law. It can be found that the difference between the acceleration and strain law of the measure points on the pile is mainly reflected in the bridge pile by the hillside.
- (4) With the increase of excitation intensity, the dominant frequency of the slope body and the bridge pile located on the slope slide gradually shifted from low frequency to high frequency, while the dominant frequency of the riverside slope did not show a tendency to change to high frequency. This is because the bridge-landslide interaction leads to the dissipation of earthquake wave energy, increases the damping of the interaction system, and prolongs its natural vibration period. Therefore, the dominant frequency at the riverside is still in the low-frequency region.
- (5) Through correlation analysis, it is found that, whether it is a bridge or a slope body, as the distance between the measuring points increases (decreases), the correlation between the measuring points decreases (increases) on the different working conditions; and the correlation between measuring points increases with the increase of earthquake waves.

In general, this paper studies the disaster mechanism of the bridge-landslide parallel system. However, there are still many aspects that need to be studied in depth. In general, the disaster mechanism of bridge-landslide parallel system is studied in this paper. However, there are still many aspects that need to be deeply studied. In the follow-up work, the author plans to compare and analyze the numerical simulation and experimental results. In the aspect of frequency, the response difference of bridge-landslide parallel system under high frequency and low frequency will be discussed more deeply. The slope stability will be studied from the selection of geotechnical parameters and soil self-weight effect.

## Data Availability

The data used to support the findings of this study are available from the corresponding author upon request.

## Conflicts of Interest

The authors declare that they have no conflicts of interest.

## Acknowledgments

This research was supported by the National Key R&D Program of China (2018YFC1504901), the Project on Science and Technology Development Project of Natural Science Foundation of Gansu Province (145RJZA068), Outstanding Postgraduate “Innovation Star” Project (2021CXZX-632), Research on Key Technology of Long Tunnel Construction in Complex Environment-Deepening Research on Deformation Mechanism (2017-KJ008-Z008-XB), and Gansu Youth Science and Technology Fund (2021-0406-JCC-0663).

## References

- [1] Y. Dong, Z. Feng, J. He, H. Chen, G. Jiang, and H. Yin, “Seismic response of a bridge pile foundation during a shaking table test,” *Shock and Vibration*, vol. 2019, pp. 1–16, 2019.
- [2] H. Wu et al., “Geological analysis and model test study on deformation mechanism of red bed landslide at longmuergou, Qinghai Plateau,” *Rock Mechanics and Engineering*, vol. 29, no. 10, pp. 2094–2102, 2010.
- [3] D. Song et al., “Dynamic response analysis of rock bank slope of a eridge across Jinsha River under earthquakes,” *Advanced Engineering Sciences*, vol. 53, no. 2, pp. 45–53, 2021.
- [4] S. Yao, K. Kobayashi, N. Yoshida, and H. Matsuo, “Interactive behavior of soil-pile-superstructure system in transient state to liquefaction by means of large shake table tests,” *Soil Dynamics and Earthquake Engineering*, vol. 24, no. 5, pp. 397–409, 2004.
- [5] K. Tokimatsu, H. Suzuki, and M. Sato, “Effects of inertial and kinematic interaction on seismic behavior of pile with embedded foundation,” *Soil Dynamics and Earthquake Engineering*, vol. 25, no. 7, pp. 753–762, 2005.
- [6] K. T. Chau, C. Y. Shen, and X. Guo, “Nonlinear seismic soil-pile-structure interactions: shaking table tests and FEM analyses,” *Soil Dynamics and Earthquake Engineering*, vol. 29, no. 2, pp. 300–310, 2009.
- [7] H. Dou and P. M. Byrne, “Dynamic response of single piles and soil-pile interaction,” *Canadian Geotechnical Journal*, vol. 33, no. 1, pp. 80–96, 1996.
- [8] X. Gao, X.-z. Ling, L. Tang, and P.-j. Xu, “Soil-pile-bridge structure interaction in liquefying ground using shake table testing,” *Soil Dynamics and Earthquake Engineering*, vol. 31, no. 7, pp. 1009–1017, 2011.
- [9] S.-C. Wang, K.-Y. Liu, C.-H. Chen, and K.-C. Chang, “Experimental investigation on seismic behavior of scoured bridge pier with pile foundation,” *Earthquake Engineering & Structural Dynamics*, vol. 44, no. 6, pp. 849–864, 2015.
- [10] M. G. Durante, L. Di Sarno, G. Mylonakis, C. A. Taylor, and A. L. Simonelli, “Soil-pile-structure interaction: experimental outcomes from shaking table tests,” *Earthquake Engineering & Structural Dynamics*, vol. 45, no. 7, pp. 1041–1061, 2016.
- [11] V. Shirgir, A. Ghanbari, and A. Massumi, “Analytical model for time history analysis of single pier bridges considering soil-pile structure interaction effects,” *Applied Mathematical Modelling*, vol. 93, pp. 257–275, 2021.
- [12] C. Zhang, G. Jiang, L. Su, D. Lei, W. Liu, and Z. Wang, “Large-scale shaking table model test on seismic performance of bridge-pile-foundation slope with anti-sliding piles: a case study,” *Bulletin of Engineering Geology and the Environment*, vol. 79, no. 3, pp. 1429–1447, 2020.
- [13] G. Luo, X. Hu, E. T. Bowman, and J. Liang, “Stability evaluation and prediction of the Dongla reactivated ancient landslide as well as emergency mitigation for the Dongla Bridge,” *Landslides*, vol. 14, no. 4, pp. 1403–1418, 2017.
- [14] C.-Y. Chen et al., “Numerical modeling of interactions of rainfall and earthquakes on slope stability analysis,” *Environmental Earth Sciences*, vol. 10, p. 8, 2021.
- [15] V. B.-Q. Nguyen and Y.-T. Kim, “Rainfall-earthquake-induced landslide hazard prediction by Monte Carlo simulation: a case study of mt. Umyeon in korea,” *KSCE Journal of Civil Engineering*, vol. 24, no. 1, pp. 73–86, 2020.
- [16] A. M. Rajabi, M. Khodaparast, and M. Mohammadi, “Earthquake-induced landslide prediction using back-propagation type artificial neural network: case study in northern Iran,” *Natural Hazards*, 2021.
- [17] S. He et al., “Research on rockfall impact prevention of Chediguan bridge pier, Duwen road,” *Chinese Journal of Rock Mechanics and Engineering*, vol. 32, no. S2, pp. 3421–3427, 2013.
- [18] C. Yan et al., “Impact analysis of creep movement of zhengjiaawan landslide to bridge across,” *Journal of Engineering Geology*, vol. 25, no. 2, pp. 416–423, 2017.
- [19] W. Yao et al., “Research on deformation mechanism and renovation technology of bridges passing through a deep landslide system,” *Journal of Engineering Geology*, vol. 26, no. S, pp. 219–226, 2018.
- [20] C. Zhou et al., “Molding simulation of soft rock based on natural red bed materials,” *Rock Mechanics and Engineering*, vol. 41, no. 2, pp. 419–427, 2020.
- [21] J. Liu, *Large-scale Model Test Study of Pipeline Crossing Landslide Interaction*, Master Thesis, Chengdu University of Technology, 2012.
- [22] B. Yang et al., “Dynamic response and failure characteristic of accumulation slope under action of different kinds of seismic load,” *China Civil Engineering Journal*, vol. 52, no. S1, pp. 202–210, 2019.
- [23] S. Hu et al., “Seismic response analysis of soil-column-free large-span metro station structure,” *Tunnel Construction*, vol. 40, no. 3, pp. 352–363, 2020.
- [24] T. Anagnos and A. S. Kiremidjian, “A review of earthquake occurrence models for seismic hazard analysis,” *Probabilistic Engineering Mechanics*, vol. 3, no. 1, pp. 3–11, 1988.
- [25] Y. Guan, *Study on Determination Method of Design Ground Motion Considering Multiple Earthquake Action*, Institute of Engineering Mechanics, China Earthquake, (in Chinese), 2015.
- [26] A. Sha, D. Yun, L. Hu, and C. Tang, “Influence of sampling interval and evaluation area on the three-dimensional pavement parameters,” *Road Materials and Pavement Design*, vol. 22, no. 9, pp. 1964–1985, 2021.
- [27] China Railway First Highway Survey and Design Research Institute Co Ltd, *JTG C20-2016 Highway Engineering Geological Survey Code*, People’s Communications Press, Beijing, China, (in Chinese), 2011.
- [28] China Railway Press, *High-speed Railway Design Code: TB10621-2014*, China Railway Press, Beijing, China, 2015.
- [29] China Building Industry Press, “Editorial board of handbook of engineering geology,” *Handbook of Engineering Geology*, China Building Industry Press, Beijing, China, (in Chinese), 5th edition, 2018.